Coupled Lasers Rotation Sensor (CLARS)

Jacob Scheuer, *Senior Member, IEEE, Member, OSA*, and Ben Z. Steinberg, *Senior Member, IEEE*

***Abstract*—We study the lasing eigen-modes and dynamics of circular array of coupled lasers in a rotating framework for ultrasensitive integrated optical rotation sensing applications. The dependence of the mode and frequency splitting on the array parameters and pumping level is studied in details. The impact of structure variations and disorder such as variations of the resonance wavelength of the individual cavities and the inter-cavity coupling is studied and found to generate a "dead-zone" which limits the sensitivity of the sensor.**

***Index Terms*—Gyroscopes, integrated optics devices, Sagnac effect.**

I. Introduction

An electromagnetic wave propagating along a circular path in a rotating medium accumulates additional phase shift which depends on the medium rotation. This phase shift, known as the Sagnac effect, is the underlying mechanism of contemporary high-resolution optical rotation sensors and Gyros. Optical rotation sensors can be roughly divided into two subcategories: 1) passive devices that generally measure the phase shift between the clockwise (CW) and counterclockwise (CCW) rotating waves using interferometric methods and 2) active devices (lasers) that measure the beating between the resonance frequencies of the CW and CCW rotating waves [1]. The detection threshold of Gyros belonging to these subcategories is limited by different mechanisms. Passive devices are basically limited by the minimal power which can be detected, which is determined by Schott noise while laser Gyros are theoretically limited by a phenomenon called injection locking which tends to lock the frequencies of the CW and CCW rotating waves at low rotation rates. This frequency locking is caused by undesired reflections and backwards scattering of one mode to the other due to imperfections in the optical path. However, the injection locking phenomenon can be eliminated by employing various techniques [1] such as biasing the Gyro using a known rotation rate, etc. As a result, laser Gyros are more commonly used then their passive counterpart, especially when the detection of very low rotation rates are desired. Nevertheless, the *responsivity*, which determines the device accuracy, of both active and passive devices is determined almost solely by the area circumvented by the optical path [2], thus necessitating relatively large devices.

Recently, the Sagnac effect was studied in slow-wave structures consisting of single and multi mode coupled micro-cavities [3], [4]. These studies demonstrated the slow-wave structure potential for responsivity enhancement while retaining compact dimensions. In particular, it was found that the Sagnac effect is manifested differently in slow-wave structure and that the responsivity is determined not only by the area of the device. Other parameters such as number of cavities, inter-cavity coupling and the area of the individual cavities play a role in determining the Gyro responsivity [3]–[5].

These studies, however, where focused on *passive* devices which exploit the difference in the phase accumulated by the CW and CCW rotating waves. Generally speaking, the performances of passive CROW based devices, particularly CROW delay lines, are inherently limited by the losses (i.e., the Q-factor) of the individual cavities [6]. Recently, it was suggested to incorporate gain into the cavity to overcome this problem [7]. Here we study *active* slow-wave rotation sensors in which each cavity is a micro-laser. A realization of such structure employing a circular array of vertical cavity surface emitting lasers (VCSELs) is depicted in Fig. 1. Unlike continuous optical path ring lasers (such as fiber lasers) the "backwards scattering" in a coupled resonator optical waveguide (CROW) structure is inherently manifested by the inter-laser coupling coefficient and does not need to be introduced phenomenologically. Another novel configuration for rotation sensing, based on radial Bragg reflection, was recently proposed and studied theoretically [8].

In Section II we present the theoretical framework and derive a set of rate equations for the circular laser array. In Section III we study the lasing modes and dynamics of the array. In Section IV we study the effect of structural variations and inaccuracy on the device performance. In Section V we discuss the results and summarize.

II. Theoretical Framework

A. The Passive CROW

We base our derivation of the passive CROW based gyroscope on the tight-binding approach, adapted to rotating systems [3]. Our CROW gyroscope consists of an array of N weakly coupled optical resonators situated along a closed circular path as shown in Fig. 1. The n-th resonator is centered at $\boldsymbol{r}_n$, and in the absence of its neighbors and under stationary conditions it is completely characterized by the (possibly complex) relative dielectric structure $\varepsilon_C(\boldsymbol{r}-\boldsymbol{r}_n)$, supporting a single optical mode with resonance frequency ω_0, with electric and magnetic fields

Manuscript received nulldate. Current version published January 28, 2009. This work was supported in part by the Israeli Science Foundation (FIRST program) and RAFAEL.

J. Scheuer is with the School of Electrical Engineering and the Center for Nanotechnology and Nanoscience, Tel-Aviv University, Tel-Aviv, Israel 69978 (e-mail: kobys@eng.tau.ac.il).

B. Z. Steinberg is with the School of Electrical Engineering, Tel-Aviv University, Tel-Aviv, Israel 69978 (e-mail: steinber@eng.tau.ac.il).

Color versions of one or more of the figures in this paper are available online at http://ieeexplore.ieee.org.

Digital Object Identifier 10.1109/JLT.2008.2004923

$\boldsymbol{E}_C(\boldsymbol{r}-\boldsymbol{r}_n), \boldsymbol{H}_C(\boldsymbol{r}-\boldsymbol{r}_n)$, respectively. These modes satisfy the standard wave equation:

$$\Theta_C \boldsymbol{H}_C = k_0^2 \boldsymbol{H}_C, \quad \Theta_C \equiv \nabla \times [1/\varepsilon_C(\boldsymbol{r})] \nabla \times, \quad k_0 = \omega_0/c \tag{1}$$

where c *is the* vacuum speed of light. Let $E_\Omega(r)$ and $H_\Omega(r)$ be the electromagnetic fields of the entire structure, under rotation. In the rotating system rest frame, H_Ω satisfies the following wave equation [3]

$$\Theta \boldsymbol{H}_\Omega = k^2 H_\Omega + ik\mathbf{L}_\Omega \boldsymbol{H}_\Omega, \ \ \Theta \equiv \nabla \times [1/\varepsilon(r)] \nabla \times, \ \ k = \omega/c \tag{2}$$

where $\varepsilon(\boldsymbol{r})$ describes the entire (relative) dielectric structure as seen when stationary. It is assumed for the moment to be ideal (i.e., without structural disorder). ω is the optical frequency, and $\mathbf{L}_\Omega$ is the rotation operator:

$$\begin{aligned} \mathbf{L}_\Omega \boldsymbol{H}_\Omega &= \nabla \times [\boldsymbol{\beta}/\varepsilon(\boldsymbol{r}) \times \boldsymbol{H}_\Omega] + \boldsymbol{\beta}/\varepsilon(\boldsymbol{r}) \times [\nabla \times \boldsymbol{H}_\Omega], \\ \boldsymbol{\beta} &= c^{-1}\Omega \hat{\boldsymbol{z}} \times \boldsymbol{r} \end{aligned} \tag{3}$$

Here Ω is the angular velocity of the structure. It should be noted that both ε and ε_C have real and imaginary parts, i.e., $\varepsilon_C = \varepsilon_C^R + i\varepsilon_C^I$, $\varepsilon = \varepsilon^R + i\varepsilon^I$. To solve (2), we adopt the extended tight binding approach and expand the total field of the rotating system using the modes of the isolated and stationary micro-cavities [3]:

$$\boldsymbol{E}(\boldsymbol{r}) = \sum_{n=1}^{N} A_n \boldsymbol{E}_C(\boldsymbol{r}-\boldsymbol{r}_n), \quad \boldsymbol{H}(\boldsymbol{r}) = \sum_{n=1}^{N} A_n \boldsymbol{H}_C(\boldsymbol{r}-\boldsymbol{r}_n) \tag{4}$$

Due to the tight-binding (weak coupling) assumption, the effect of inter cavity coupling, as well as the effect of rotation, are manifested essentially via the (yet unknown) expansion coefficients A_n. Note that the relevant wave equation for the total field (2) is no longer self adjoint (due to rotation), thus the variational solution procedure usually employed in tight-binding theory cannot be invoked. Instead, we introduce (4) and (1) into (2) and multiply both sides by $H_C^*(\boldsymbol{r}-\boldsymbol{r}_m)$, keeping only the exponentially dominant terms (nearest neighbor coupling). The result is the matrix equation for the field expansion coefficients $A_m (m = 1 \ldots N)$:

$$\begin{aligned} \Delta\omega A_m(1-i\delta) = {} & \frac{1}{2}\omega_0|\kappa_1|e^{i\varphi_\kappa}(A_{m-1}+A_{m+1}) \\ & -\frac{1}{2}\omega_0 A_m \Delta\alpha e^{i\varphi_{\Delta\alpha}} + i\Omega\gamma_1(A_{m+1}-A_{m-1}) \end{aligned} \tag{5}$$

where we assume $\omega \approx \omega_0$, define $\Delta\omega = \omega - \omega_0$ and

$$\begin{aligned} \kappa_1 = {} & \frac{-1}{\eta_0^2 I_0} \int_{V_1} \Delta\varepsilon_C(\boldsymbol{r}-\boldsymbol{r}_1) \frac{\varepsilon_C(\boldsymbol{r}-\boldsymbol{r}_2)\varepsilon_C^*(\boldsymbol{r}-\boldsymbol{r}_1)}{\varepsilon_b(\boldsymbol{r})\varepsilon_C(\boldsymbol{r}-\boldsymbol{r}_1)} \\ & \cdot \boldsymbol{E}_C(\boldsymbol{r}-\boldsymbol{r}_2) \cdot \boldsymbol{E}_C^*(\boldsymbol{r}-\boldsymbol{r}_1) d^3r \\ \Delta\alpha = {} & 2\tilde{\tau}_0^R/\eta_0^2 I_0 \\ \delta = {} & \omega_0 \tilde{\tau}_0^I/\eta_0^2 I_0 \\ \tilde{\tau}_0 = {} & \tilde{\tau}_0^R + i\tilde{\tau}_0^I \\ = {} & -\int_{V_{m+1}} \frac{\Delta\varepsilon_C(\boldsymbol{r}-\boldsymbol{r}_{m+1})}{\varepsilon_b(\boldsymbol{r})\varepsilon_C(\boldsymbol{r}-\boldsymbol{r}_{m+1})} \\ & \times |\varepsilon_C(\boldsymbol{r}-\boldsymbol{r}_m)\boldsymbol{E}_C(\boldsymbol{r}-\boldsymbol{r}_m)|^2 d^3r \end{aligned}$$

$$\begin{aligned} I_0 = {} & \int |\boldsymbol{H}_C|^2 d^3r \\ \eta_0^2 = {} & \mu_0/\varepsilon_0 \\ \gamma_1 = {} & \frac{1}{I_0} \int \frac{|\boldsymbol{r}|}{\varepsilon(\boldsymbol{r})} \hat{\boldsymbol{\varphi}} \\ & \cdot \{\boldsymbol{H}_C(\boldsymbol{r}-\boldsymbol{r}_1) \times [\nabla \times \boldsymbol{H}_C(\boldsymbol{r}-\boldsymbol{r}_2)]\}^* d^3r \end{aligned} \tag{6}$$

In the above V_m is the volume of the mth cavity, $\varepsilon_\mathrm{b}(\boldsymbol{r})$ is the dielectric property of the background medium (the medium when the optical resonators are absent) and $\Delta\varepsilon_\mathrm{C}(\boldsymbol{r}-\boldsymbol{r}_n) = \varepsilon_\mathrm{C}(\boldsymbol{r}-\boldsymbol{r}_n) - \varepsilon_\mathrm{b}(\boldsymbol{r})$ is the contrast property created by the presence of the nth cavity. These expressions are directly obtained from their generic definitions in [3] [see Eqs (2.7'), (2.9') and (2.22')], with some algebraic simplifications due to the fact that the modal fields $\boldsymbol{E}_C(\boldsymbol{r}-\boldsymbol{r}_n), \boldsymbol{H}_C(\boldsymbol{r}-\boldsymbol{r}_n)$ are associated with stationary and isolated single resonator, e.g., $\nabla \times \boldsymbol{H}_C(\boldsymbol{r}-\boldsymbol{r}_n) = -i\omega_0\varepsilon_0\varepsilon_C(\boldsymbol{r}-\boldsymbol{r}_n)\bar{\boldsymbol{E}}_C(\boldsymbol{r}-\boldsymbol{r}_n)$, etc... It is interesting to note that, due to the last equality, the expression for the rotation coupling coefficient γ_1 is associated with the power circulating in the CROW ring due to the mutual cavity coupling. This coefficient represents the manifestation of the Sagnac effect in systems for which the optical signal cannot be expressed merely as a geometric ray or a fiber mode. See [3] and [10] for more detailed discussions.

We assume that $\delta \ll 1$ and thus the coefficient multiplying A_m on the LHS of (8) merely introduces a negligible phase shift. The assumption is valid because in all practical devices (lasers) $\varepsilon^I \ll \varepsilon^R$. $\Delta\alpha$ is also, in principle, complex but its impact can be divided into a frequency shift (the real part) and gain shift (imaginary part) for each individual laser and, thus, can be absorbed into the resonance frequency and cavity loss of each laser. Therefore, the only significant contribution stemming for the imaginary part of the refractive index is expressed in ϕ_κ (nearest neighbor coupling). Note that in the case of pure gain guided lasers $|\kappa_1|\mathrm{e}^{\mathrm{i}\phi\kappa}$ is a purely imaginary number ($\phi_\kappa = \pi/2$) and, therefore, this phase cannot be neglected.

B. The Active CROW Rate Equations

To derive the rate equations for temporal evolution of the slowly varying field envelope of E we assume the following: The time dependent amplitude of the field in each cavity can be represented by a Fourier integral—$A_m(t) = \int \hat{A}_m(\omega)\exp(i\omega t)d\omega$. This amplitude is assumed to have a relatively narrow bandwidth around ω_0, i.e., $A_m(t) = E_m(t)\exp(i\omega_0 t)$ and $E_m(t) = \int \hat{E}_m(\Delta\omega)\exp(i\Delta\omega t)d\Delta\omega$ where $\Delta\omega = \omega - \omega_0$. By inverse Fourier transforming (4), we get the following set of coupled ordinary differential equations describing the temporal evolution of the field in each micro-laser:

$$\begin{aligned} \frac{dE_m}{dt} = {} & \frac{1}{2}i\omega_0\kappa_1 e^{i\phi_\kappa}(E_{m-1}+E_{m+1}) \\ & -\frac{1}{2}i\omega_0 E_m \Delta\alpha - \Omega\gamma_1(E_{m+1}-E_{m-1}) \end{aligned} \tag{7}$$

The frequency shift term due to the self-coupling coefficient $\Delta\alpha$ can be eliminated from (7) by substituting $E_m(t) = \widetilde{E}_m(t)\exp(-(1/2)i\omega_0\Delta\alpha \cdot t)$. Similarly, the imaginary part of $\Delta\alpha$ can be absorbed into the photon lifetime. Next,

we introduce the cavity photon lifetime and the gain into (7), as well as, the rate equation for the carrier population inversion:

$$\begin{aligned}\frac{d\widetilde{E}_m}{dt} &= \frac{1}{2}\left[G(N_m) - \tau_p^{-1}\right](1+iR)\widetilde{E}_m \\ &\quad + \frac{1}{2}i\omega_0\kappa_1 e^{i\phi_\lambda}(\widetilde{E}_{m-1} + \widetilde{E}_{m+1}) \\ &\quad - \Omega\gamma_1(\widetilde{E}_{m+1} - \widetilde{E}_{m-1}) \\ \frac{dN_m}{dt} &= P - N_m\tau_s^{-1} - G(N_m)|\widetilde{E}_m|^2 \end{aligned} \tag{8}$$

where N_m is the excess carriers in laser m, P is the pump level, τ_p and τ_s are correspondingly the photons and carriers lifetimes and R is the linewidth enhancement factor connecting the change in the gain level of the semiconductor material with the change in it refractive index. $G(N_m)$ is the optical gain in laser m given by: $G(N_m) = G(N_m) + g\cdot(N_m - N_{th})$ where g is the differential gain $\partial G/\partial N$ at threshold and $G(N_{th}) = 1/\tau_p$. Finally, we normalize the rate equations according to the conventions of [9]: $A_m = \sqrt{(1/2)g\tau_s}E_m$, $Z_m = N_{th}g\tau_p(N_m/N_{th} - 1)/2$, $p_m = N_{th}g\tau_p(P_m/P_{th} - 1)/2$ where $P_{th} = N_{th}/\tau_s$, $\eta = \omega_0\tau_p\kappa_1/2$, $\eta_1 = \tau_p\gamma_1$, $T = \tau_s/\tau_p$, and $\tau = t/\tau_p$. Introducing the normalized variables to (7) yields the following normalized rate equations:

$$\begin{aligned}\dot{A}_m &= Z_m(1+iR)A_m + i\eta e^{i\phi_\eta}(A_{m+1} + A_{m-1}) \\ &\quad - \eta_1\Omega(A_{m+1} - A_{m-1}) \\ T\cdot\dot{Z}_m &= p_m - Z_m - (1+2Z_m)|A_m|^2 \end{aligned} \tag{9}$$

where the dot indicates a derivative with respect to τ. For a circular array consisting of L lasers the boundary conditions are $A_0 = A_L$ and $A_{L+1} = A_1$. (9) possesses the functional form of the conventional rate equations but with an additional term which is linearly dependent on the mechanical rotation rate, Ω and a new coupling coefficient, η_1, defined by the overlap integral in (6).

III. The Lasing Modes in the Rotating Framework

A. The Responsivity

To study the dynamics and lasing properties of the circular arrays subjected to mechanical rotation, (9) were solved numerically using a forth order Runge–Kutta integration scheme [7]. For simplicity it was initially assumed that the two coupling coefficients between adjacent micro-lasers (η and η_1) and the pumping levels (p_m) are identical for all the lasers in the array. An array consisting of L lasers has L eigen-modes of which $L-1$ $(L-2)$ are degenerate for an odd (even) L. The degenerate modes correspond to CW and CCW rotating waves. The nondegenerate modes of the array are the in-phase (no phase shift between adjacent lasers) and the anti-phase (π phase shift between adjacent lasers) modes which are stationary (standing waves). In should be noted that, in a circular array of odd L the anti-phase mode does not exist due to phase frustration [12] and, therefore, for such arrays there is only a single nondegenerate eigen-mode.

For rotation sensing applications we are interested in the beating frequency generated due to the rotation induced splitting of originally degenerate CW and CCW rotating modes. Therefore, the nondegenerate solutions are unusable (see e.g., [10] and [11] for a general discussion on the role of mode-degeneracy under rotation). However, it is well known that (nondegenerate) anti-phase mode tends to be the dominant lasing solution in coupled laser arrays, having the lowest lasing threshold [13]. On the other hand, the in-phase mode generally has the highest threshold level and is seldom exhibited unless specific arrangements are made [13]. Therefore, in order to suppress the anti-phase lasing mode, it is advantageous to use an array of odd number of lasers.

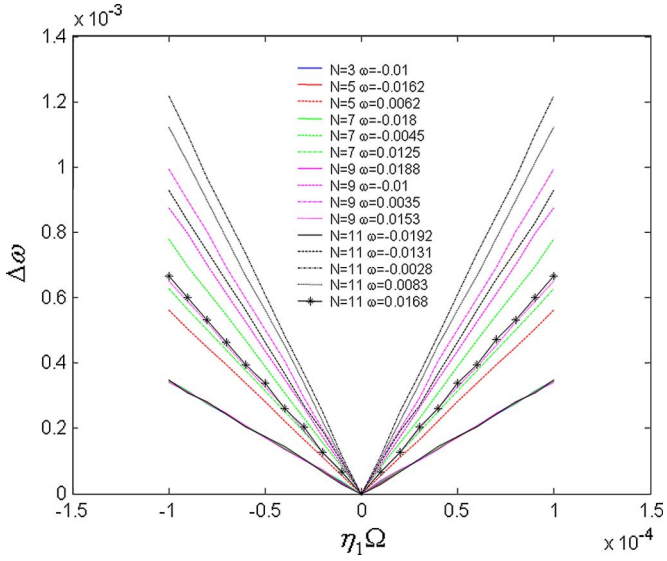

Fig. 2. Beating frequency of the different modes of CROW Gyro with 3–11 cavities. $R = 0, p = 0.1$ and $T = 300$. The parameter w indicates the specific resonance frequency of each CROW mode $w = (\omega - \omega_0)/\omega_0$.

Fig. 2 depicts the (normalized) beating frequency as a function of the (normalized) rotation rate for the various lasing modes of circular arrays consisting of 3–11 micro-lasers. The coupling coefficient $\eta = 0.01$ is identical for all the arrays and $-10^{-4} < \eta_1\Omega < 10^{-4}$. The rest of the parameters are defined in the figure caption. Each curve in the figure corresponds to the rotation induced frequency difference of originally degenerate CW and CCW rotating waves, and is designated by the (normalized) frequency shift of the degenerate modes (i.e., at $\Omega = 0$) from the resonance frequency of the individual cavity.

Fig. 2 illustrates several important properties of the active CROW rotation sensor. The responsivity of Gyro, represented by the slope of the curves, is mode dependent, i.e., each (originally) degenerate mode exhibits different splitting when subjected to rotation. As can be expected, the mode with highest sensitivity is the one for which the resonance frequency is closest to that of the individual laser. This is because the slope of the dispersion relation is steepest at this point. Another prominent characteristic is the increase in the responsivity for larger array. This trend is not surprising as it stems directly from the corresponding increase in the device area (assuming the inter-laser distance remains constant).

B. The Impact of the Pumping Level

The rate (9) describing the evolution of the field amplitude and carrier population inversion in each laser are inherently nonlinear due to the dependence of the optical gain on the field in-

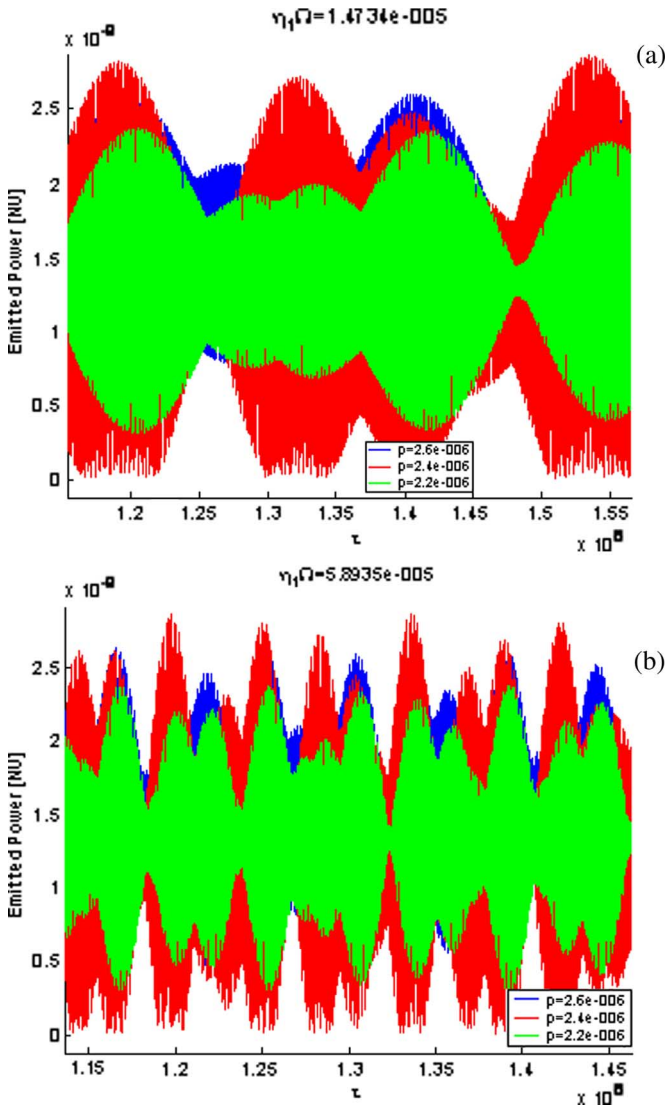

Fig. 3. Temporal evolution of the intensity as a function of the pumping level. (a) $\eta_1\Omega = 1.4734 \times 10^{-5}$; (b) $\eta_1\Omega = 5.8935 \times 10^{-5}$.

tensity. As a result it can be expected that the responsivity of an active CROW rotation sensor is affected by the pumping level.

Fig. 3 shows the temporal evolution of the intensity in one of the lasers in an odd circular array as a function of the pumping level *while the device is rotating* in various angular velocities. Two important features can be observed from Fig. 3: 1) higher pumping level results in higher output power and 2) the amplitude of the RF beating signal depends on the pumping level nonmonotonically. While the first characteristic is quite obvious, it is the second one which is rather unexpected. The ability to detect rotation in this scheme relies on the ability to detect the beating frequency between the CW and CCW rotating waves. This ability is determined by the RF measurement apparatus frequency response but also by the overall power of the signal. Increasing the pumping level increases the overall output but decreases the fractional part of the RF beating signal. It can, therefore, be expected that there exists an optimal pumping level taking into account the tradeoff between these effects. Fig. 4 shows the dependence of the beating-signal

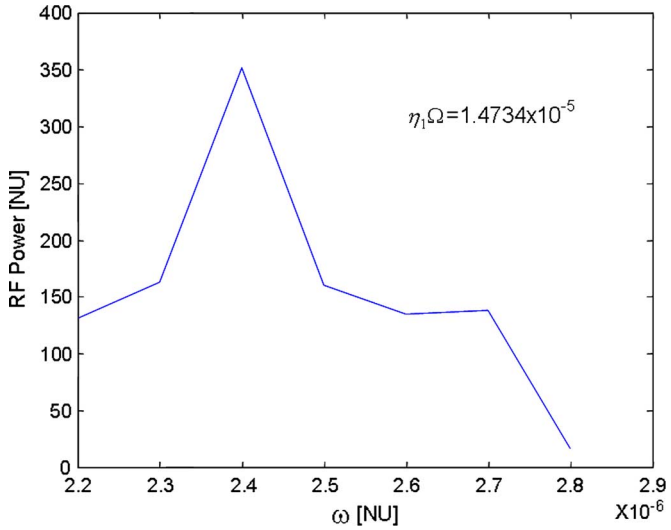

Fig. 4. Steady state RF power for $\eta_1\Omega = 1.4734 \times 10^{-5}$.

power on the pumping rates for $\eta_1\Omega = 5.8935 \times 10^{-5}$. The dependence of the emitted RF power on p for other rotation rates is nearly identical. The existence on an optimal pumping level is evident—the beating signal is maximal for $p = 2.4 \times 10^{-6}$ for all rotation rates. At this point it is not clear what the exact mechanism determining the optimal p is and although this mechanism is important and interesting, its study and identification is beyond the scope of this paper. Nevertheless, the existence of this optimal pumping level indicates that in order to enhance the sensitivity of the rotation sensor it is necessary to identify the optimal pumping for the given structure.

IV. Structure Variations—The Formation of a Dead-Zone

In any realization of these new rotation sensors, structural disorder (e.g., due to limited fabrication accuracy) may introduce new factors that are not present in the idealized geometries. Hence, the purpose of this section is to investigate the effect of structural disorder on the ED of rotating CROWs. Our study applies to the basic schemes shown in Fig. 1. We start our analysis by noting that although each individual micro-cavity does not support mode-degeneracy under stationary conditions $(\Omega = 0)$, the *entire* ideal structure does. At any given frequency within its transmission band and in the absence of structural disorder, it supports at least two optical signals: a clock-wise (CW) and a counter-clock-wise (CCW) propagating mode. Alternatively, since any linear combination of degenerate modes is by itself a degenerate mode, these modes can be equally well presented as two *real* standing waves. When the structure rotates, the corresponding degenerate resonance splits into two distinct resonances [10]. Similarly, structural disorder splits mode degeneracy. Thus, one can invoke the theory of mode-degeneracy under rotation, and extend it to hold also under structure inaccuracy using essentially the tools of [11]. This combined approach has three important advantages. First, it enables one to obtain quickly the general expression for the effect of rotation *and* structure inaccuracy on the mode splitting, where the fact that each global mode can be expressed as a summation of the

form of tight binding theory is done at a later stage, and is used only to get more explicit final results pertaining to the gyroscope dead-zone. Second, it enables one to express the structure variation using its most fundamental form—the variation of ε, while its manifestation as variation of the individual cavity resonances and its effect on the gyro dead-zone "pops out" later as derived results. Finally, this approach also reveals an interesting physical picture of two competing effects: both, structure inaccuracy and mechanical rotation break the mode degeneracy and cause resonance splitting. Splitting due to the former is Ω-independent, while splitting due to the latter scales linearly with Ω. The device can be used as a gyroscope only when the splitting due to rotation exceeds the splitting due to structure inaccuracy. Hence, a dead-zone in Ω is formed. This novel physical effect of competing processes is derived analytically and backed up by numerical simulations.

A. Theoretical Analysis

Let $\boldsymbol{H}_\Omega$ and $\boldsymbol{E}_\Omega$ be the magnetic and electric fields of the entire structure, under rotation and *structural disorder*. It satisfies the wave equation (2), (3) where $\varepsilon(\boldsymbol{r})$ describes now the entire dielectric structure, including structural disorder. At rest, and in the absence of structural disorder, the two degenerate modes $\boldsymbol{H}_0^{(m)}(\boldsymbol{r})(m=1,2)$ of the *entire* structure satisfy:

$$\Theta_0 \boldsymbol{H}_0^{(m)} = k_U^2 \boldsymbol{H}_0^{(m)},\ \ \Theta_0 \equiv \nabla \times [1/\varepsilon_U(\boldsymbol{r})]\nabla\times,\ \ k_U = \omega_U/c \tag{10}$$

where $\varepsilon_U(\boldsymbol{r})$ describes the entire *unperturbed* structure and ω_U is the corresponding resonance frequency. As shown below, rotation and structural disorder causes it to split into two different resonances. Since Θ_0 is self-adjoint $\boldsymbol{H}_0^{(m)}(\boldsymbol{r})$ can always be presented as real and orthogonal set. Also, we write:

$$\begin{aligned}\Theta &= \Theta_0 + \delta\Theta,\ \delta\Theta = \nabla \times (\delta\,[1/\varepsilon(\boldsymbol{r})])\nabla\times \\ \delta\,[1/\varepsilon(\boldsymbol{r})] &= \varepsilon^{-1}(\boldsymbol{r}) - \varepsilon_U^{-1}(\boldsymbol{r})\end{aligned} \tag{11}$$

so the wave equations (2)–(3) pertaining now to rotating and disordered structure, can be written as [neglecting higher order terms proportional to $\Omega\delta(1/\varepsilon)$]:

$$\Theta_0 \boldsymbol{H}_\Omega - k^2 \boldsymbol{H}_\Omega = (ik\mathbf{L}_\Omega^U - \delta\Theta)\boldsymbol{H}_\Omega \tag{12}$$

where $\mathbf{L}_\Omega^U$ is defined as in (3), but with $\varepsilon(\boldsymbol{r})$ replaced by the unperturbed structure $\varepsilon^U(\boldsymbol{r})$

Clearly, the LHS of (12) is nothing but the conventional wave equation governing the field in the stationary and unperturbed structure. The RHS describes two effects; that of rotation and that of structural disorder. Following a similar analysis to [10] with the exception that an additional term (structural disorder) appears in the RHS, the total field is a summation over $H_0^{(n)}(\vec{r})$ serving merely as building blocks:

$$\boldsymbol{H}_\Omega(\boldsymbol{r}) = \sum_{n=1}^{2} a_n \boldsymbol{H}_0^{(n)}(\boldsymbol{r}) \tag{13}$$

We substitute this expansion into (12), use (10), perform inner product of the resulting equation with $\boldsymbol{H}_0^{(m)}$ and use their mutual orthogonality. The result is the following 2×2 matrix-eigenvalue equation for the expansion coefficients α_n and frequency splitting $k - k_U$

$$\begin{bmatrix} D_{11} & D_{12} \\ D_{21} & D_{22} \end{bmatrix} \begin{bmatrix} a_1 \\ a_2 \end{bmatrix} = 2k_U(k-k_U) \begin{bmatrix} a_1 \\ a_2 \end{bmatrix} \tag{14}$$

where

$$\begin{aligned} D_{mn} &= -ik_U\left(\mathbf{L}_\Omega \boldsymbol{H}_0^{(n)}, \boldsymbol{H}_0^{(m)}\right) + \left(\delta\Theta \boldsymbol{H}_0^{(n)}, \boldsymbol{H}_0^{(m)}\right) \\ &= k_U^2 \Omega B_{mn} + d_{mn} \end{aligned} \tag{15a}$$

and where (f,g) is the $L_2(\mathrm{R})$ inner-product. Clearly, the two different eigenvalues of the equation above represent the frequency splitting. The coefficients B_{nm} here are due to the first inner product in (15). After some algebraic manipulations they can be expressed as

$$\begin{aligned} B_{mn} &= \varepsilon_0\left(\hat{\boldsymbol{z}}\times\boldsymbol{r}, \boldsymbol{H}_0^{(n)*}\times\boldsymbol{E}_0^{(m)} + \boldsymbol{H}_0^{(m)}\times\boldsymbol{E}_0^{(n)*}\right) \\ d_{mn} &= \left(\delta\Theta\boldsymbol{H}_0^{(n)}, \boldsymbol{H}_0^{(m)}\right) \end{aligned} \tag{15b}$$

The coefficients B_{mn} depend only on the perfect (unperturbed) structure and form a skew-symmetric imaginary matrix, with $B_{11} = B_{22} = 0$. It increases linearly with the radius of the structure. d_{mn} depend only on $\delta\Theta$ and therefore represent only structure disorder effects. By careful examination one can show that $d_{12} = d_{21}$ and $d_{11} + d_{12} \to 0$ as the number of (statistically independent) micro-cavities comprising the entire structure, increases. By solving algebraically for the eigenvalues of (14) we are left with the following analytical expression for the frequency splitting:

$$\begin{aligned} k(\Omega) - k_U &= \pm\frac{k_U}{2}|B_{12}|\sqrt{\Omega_d^2 + \Omega^2} \\ \Omega_d &= \sqrt{d_{12}^2 - d_{11}d_{22}}/k_U^2|B_{12}| \end{aligned} \tag{16}$$

Thus, the splitting versus Ω clearly possesses the form of Hyperbola, with a "dead-zone" Ω_{d} originating from the "competition" between disorder-induced splitting and rotation-induced splitting. The d_{mn} coefficients, responsible for the dead-zone extent, are related to the variance of the individual cavity resonance frequency. This is shown by expanding each of the (doubly-degenerate) modes of the entire stationary and unperturbed structure $\boldsymbol{H}_0^{(m)}(\boldsymbol{r})$, with the modes $H_C(\boldsymbol{r}-\boldsymbol{r}_j)$ of the N isolated unperturbed and stationary micro-cavities in the structure (consistent with tight-binding theory, described in Section III above), and with expansion coefficients c_j that should satisfy the CROW dispersion relation at rest (in fact, they are given by the A_n of (4) at $\Omega = 0$; there are two possible solutions)

$$\boldsymbol{H}_0^{(m)} = \sum_{j=1}^{N} c_j^m(\omega)\boldsymbol{H}_C(\boldsymbol{r}-\boldsymbol{r}_j) \tag{17}$$

By definition, the modal field of the j-th cavity, $\boldsymbol{H}_C(\boldsymbol{r}-\boldsymbol{r}_j)$, satisfies (1) with $\varepsilon_C(\boldsymbol{r})$ replaced by $\varepsilon_C(\boldsymbol{r}-\boldsymbol{r}_j)$. Substituting (17)

into the d_{mn} definition (15a), using (1) shifted to the jth position, using also the fact that $\nabla \times \boldsymbol{H}_C(\boldsymbol{r}-\boldsymbol{r}_j) = -i\omega_0\varepsilon_0\varepsilon_C(\boldsymbol{r}-\boldsymbol{r}_j)\boldsymbol{E}_C(\boldsymbol{r}-\boldsymbol{r}_j)$, and that $\boldsymbol{E}_C(\boldsymbol{r}-\boldsymbol{r}_j)$ is highly localized within the jth micro-cavity, we end up with

$$d_{mn} = \omega_0^2\varepsilon_0^2 \sum_{j=1}^{N} c_j^n c_j^m \left(\delta\varepsilon_C^j \boldsymbol{E}_j, \boldsymbol{E}_j\right)$$
$$= 2k_0 c^{-1} \|\boldsymbol{H}_0\|^2 \sum_{j=1}^{N} c_j^n \overline{c}_j^m \delta\omega_j \qquad (18)$$

where $\delta\varepsilon_C^j$ is the variation of the dielectric structure of the j-th resonator due to structural disorder, and $\boldsymbol{E}_j = \boldsymbol{E}_C(\boldsymbol{r}-\boldsymbol{r}_j)$. The last equality above is due to cavity perturbation theory [11], [14], and $\delta\omega_j$ is the deviation of the j-th micro-cavity resonant frequency due to structural disorder. Hence, one can relate the statistics of the individual resonances variations to the dead-zone extent. Our analysis reveals an important phenomenology. Note that (18) depends only on the disorder statistics, while B_{mn} in (15b) increases linearly with the gyroscope size [10] (note the $\boldsymbol{r}$ vector within the inner product). Therefore, for a given level of structural disorder, the dead-zone Ω_{d} in (16) decreases as the gyroscope size increases; the effect of scattering does not "add up" as one uses more micro-cavities in the gyro. In adds up only when disorder increases.

B. Numerical Results

A numerical statistical analysis of the impact of fabrication errors was performed for a 7-cavity circular CROW. The coupling coefficient between adjacent cavities was set to be $\eta = 0.01$ and the normalized rotation rate is scanned between $-10^{-4} < \eta_1\Omega < 10^{-4}$. For an ideal structure (all cavities having identical resonance frequency) the stationary system has four resonance frequencies where three of them are doubly degenerate. Under rotation the degeneracy is lifted and a beat signal between the originally degenerate modes is formed. Fig. 5 shows the frequency of the beat signal of an ideal system undergoing rotation. The three lines correspond to the three different degenerate modes.

Fabrication errors are modeled by introducing shifts (deviations) in the resonance frequencies of the individual cavities. The deviations lift the degeneracy of the modes and, as a result, there is a beat frequency even without rotation. More over, at low rotation rates the sensitivity of the Gyro is reduced. The differences between the resonance frequencies of the cavities comprising the CROW are assumed to be normally distributed with variance σ. Fig. 6 shows the frequency of the beat signal of a "realistic" CROW Gyro with $\sigma = 10^{-3}$.

The stars indicate the numerically calculate beat frequency while the solid line represent a fit to hyperbola—$\Delta\omega_{\mathrm{beat}} = \sqrt{a^2 + b^2(\eta_1\Omega)^2}$. Fig. 6 illustrates the decrease of the Gyro sensitivity for lower rotation rates. The excellent agreement of the numerical data to the hyperbolic fit (as predicted by the analysis of Section IV-A) enables the extraction of the sensitivity (the slope of the linear parts of the hyperbola) and the "dead-zone"—the minimal rotation rate that can be detected by the Gyro.

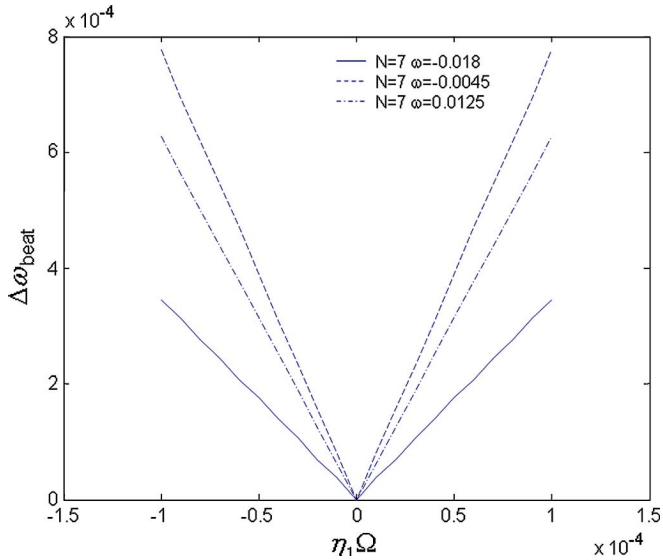

Fig. 5. Beating frequencies of an ideal rotating CROW consisting of seven cavities. The parameters are as in Fig. 2.

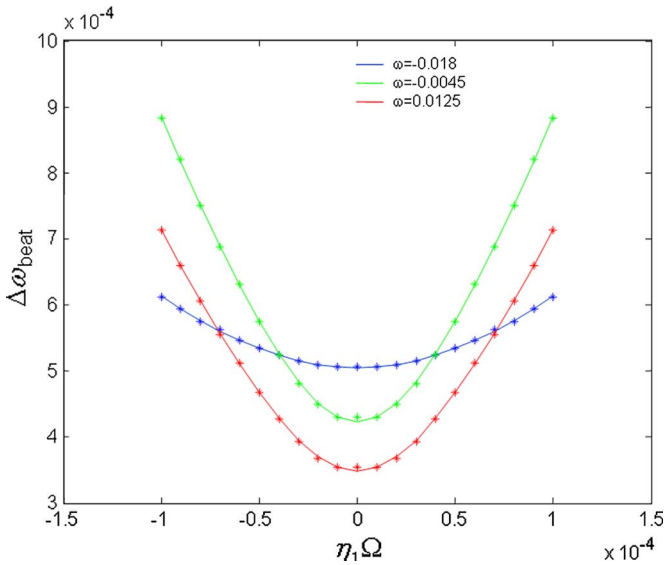

Fig. 6. Beating frequencies of a realistic rotating CROW consisting of seven cavities. The parameters are as in Fig. 2, the standard deviation of resonance of the individual cavities is $\sigma = 10^{-3}$.

An intuitive method to define the sensitivity is to calculate at the slope of hyperbola:

$$\frac{d\omega_{beat}}{d(\eta_1\Omega)} = \frac{b}{\sqrt{1 + (a/b)^2 \cdot (\eta_1\Omega)^{-2}}} \qquad (19)$$

For large rotation rate the slope is almost constant but when $\eta_1\Omega$ becomes smaller than a/b the slope starts to decrease. Therefore, it is reasonable to define the minimal detectable (normalized) rotation rate as $(\eta_1\Omega)_{\min} = a/b$, where a and b are the hyperbola parameters found from the fit.

The statistical analysis was performed by evaluating the sensitivity and dead-zone for σ ranging between 10^{-3} and 5×10^{-3} (in the normalized time units). For each σ, 10 different structures where analyzed and the average slope and $(\eta_1\Omega)_{\min}$ were

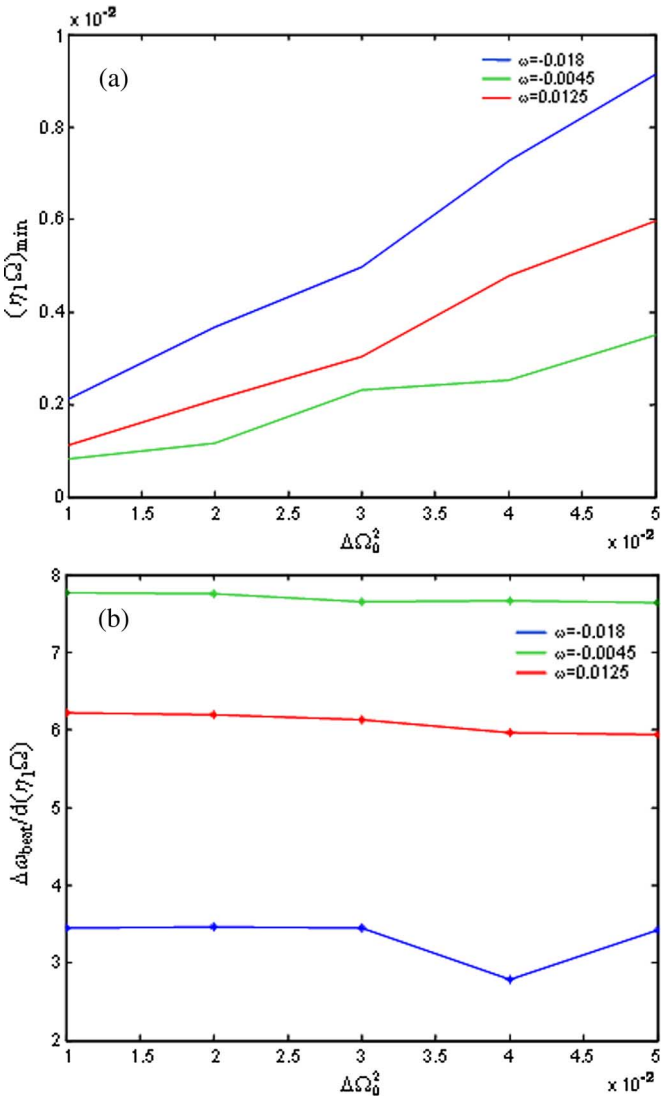

Fig. 7. Dead-zone (a) and sensitivity (b) of a "realistic" CROW as a function of σ. The rest of the parameters are as in Fig. 2.

found for each of the three beat signals. Fig. 7 depicts the average dead-zone (a) and the sensitivity (b) for different σ.

Two points that are clearly indicated in Fig. 7 The sensitivity is relatively independent of the fabrication errors—only a minor decrease of the slope is observed when the resonance frequency variance is increased. The dead-zone, on the other hand, increases significantly as σ is increased. Similar increase in the dead-zone is found for the three different modes.

It should be emphasized that despite the different underlying mechanism of the dead-zone observed in conventional laser gyros (back scattering), the physics is similar. In both cases the ideal degeneracy between the CW and CCW propagating modes is removed and the Sagnac effect must exceed the frequency splitting in order to be observed.

However, as the number of laser composing the gyro is increased *while keeping structural disorder at a constant level*, the dead-zone decreases and the minimal detected rotation rate is reduced (see Fig. 8). The reason for this phenomenon, which is in contrast to conventional gyros in which larger loops increase the

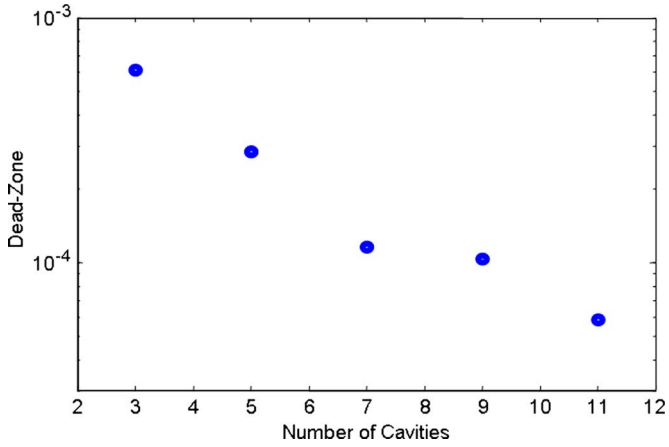

Fig. 8. The dependence of the dead-zone on the number of lasers comprising the array.

dead-zone, stem from (16) and (18). The coefficient d_{mn} defined in (18) are determined by the variations in the resonance frequencies caused by the structural disorder while $|B_{12}|$ defined in (15b) increases linearly with the structure average radius (or, equivalently, with the number of lasers). Consequently, as we increase the number of laser comprising the array dead-zone, Ω_d, decreases.

V. Discussion and Summary

Closed loop slow light structures based on coupled micro cavities form a novel approach for the realization of ultra-compact, chip level, rotation sensors. The incorporation of optically active cavities (i.e., lasers) can counteract the impact of optical loss (existing in passive structures) which is the main factor limiting the achievable sensitivity in CROW rotation sensors. We studied the dynamical behavior of closed-loop coupled laser arrays under mechanical rotation with applications to sensing. We found that fabrication tolerances generate a "dead-zone", similar to that found in conventional laser gyros, which depends on the variations of the individual lasers. This dead-zone is formed because the originally degenerate modes of the circular arrays split in the presence of fabrication errors. This splitting limits the minimal rotation rate that can be detected by the gyro (the rotation induced frequency different must exceed the original splitting).

However, we have shown that expect that as we increase the number of laser composing the gyro *while keeping structural disorder at a constant level*, the dead-zone decreases and the minimal detected rotation rate is reduced. Hence, the CLARS structure provides an inherent mechanism to arbitrarily reduce the dead-zone without necessitating enhanced fabrication capabilities.

References

[1] S. Ezekiel, *Optical Fiber Rotation Sensing*, W. K. Burns, Ed. Boston: Academic, 1994.
[2] H. J. Arditty and H. C. Lefevre, "Sagnac effect in fiber gyroscopes," *Opt. Lett.*, vol. 6, pp. 401–403, 1981.
[3] B. Z. Steinberg, "Rotating photonic crystals: A medium for compact optical gyroscopes," *Phys. Rev. E*, vol. 71, p. 056621, 2005.

[4] J. Scheuer and A. Yariv, "Sagnac effect in coupled resonator slow light waveguide structures," *Phys. Rev. Lett.*, vol. 96, p. 053901, 2006.
[5] B. Z. Steinberg, J. Scheuer, and A. Boag, "Rotation-induced superstructure in slow-light waveguides with mode-degeneracy: Optical gyroscopes with exponential sensitivity," *J. Opt. Soc. Amer. B.*, vol. 24, pp. 1216–1224, 2007.
[6] J. Scheuer, G. T. Paloczi, J. K. S. Poon, and A. Yariv, "Coupled resonator optical waveguides: Towards slowing and storing of light," *Opt. Photon. News*, vol. 16, pp. 36–40, 2005.
[7] J. Scheuer, "Slow propagation of externally injected light pulses in coupled semiconductor laser array," *Europhys. Lett.*, vol. 77, p. 44004, 2007.
[8] J. Scheuer, "Direct rotation-induced intensity modulation in circular Bragg micro-lasers," *Opt. Exp.*, vol. 15, p. 15053, 2007.
[9] S. S. Wang and H. G. Winful, "Dynamics of phase-locked semiconductor laser arrays," *Appl. Phys. Lett.*, vol. 52, pp. 1774–1776, 1986.
[10] B. Z. Steinberg and A. Boag, "Splitting of microcavity degenerate modes in rotating photonic crystals—The miniature optical gyroscopes," *J. Opt. Soc. Amer. B*, vol. 24, no. 1, pp. 142–151, 2007.
[11] B. Z. Steinberg, A. Boag, and R. Lisitsin, "Sensitivity analysis of narrowband photonic crystal filters and waveguides to structure variationas and inaccuracy," *J. Opt. Soc. Amer. A.*, vol. 20, no. 1, pp. 138–146, 2003.
[12] T. Fishman and M. Orenstein, "Cyclic vertical cavity semiconductor laser arrays with odd numbers of elements: Lasing modes and symmetry breaking," *Opt. Lett.*, vol. 21, no. 8, pp. 600–602, 1996.
[13] H.-J. Yoo, J. R. Hayes, E. G. Paek, A. Scherer, and Y.-S. Kwon, "Array mode analysis of two-dimension phased arrays of vertical cavity surface emitting lasers," *IEEE J. Quantum Electron.*, vol. 26, no. 7, pp. 1039–1051, Jul. 1990.
[14] R. F. Harrington, *Time Harmonic Electromagnetic Fields*. New York: McGraw-Hill, 1961.

Jacob Scheuer (S'99–M'01–SM'06) received the B.Sc. degree (*summa cum laude*) in electrical engineering and physics and the Ph.D. degree in electrical engineering from Technion-Israel Institute of Technology, Haifa, Israel, in 1993 and 2001, respectively.

He was a Chief Designer with Lambda Crossing, an optical component startup specializing in microring resonators for two years. Then, he joined the Center for the Physics of Information and the Department of Applied Physics, California Institute of Technology, Pasadena, as a Research Associate. Currently, he is a Senior Lecturer with the School of Electrical Engineering, Tel-Aviv University, Ramat-Aviv, Tel-Aviv, Israel. His research interests include nanophotonics, polymer optics, slow light, and secure communications.

Dr. Scheuer is a member of the Optical Society of America.

Ben Z. Steinberg (SM'99) received the Ph.D. degree in electrical engineering from Tel-Aviv University, Ramat-Aviv, Tel-Aviv, Israel, in 1989.

From 1989 to 1991, he was a Research Scholar with the Catholic University of America, Washington, DC. In 1991, he joined the faculty of engineering at Tel-Aviv University, where he is currently a Professor of electrical engineering. His main research interests are electromagnetic theory, wave propagation, and photonic and RF devices.